ChemPubSoc Europe

DOI: 10.1002/chem.201705362

CHEMISTRY A European Journal Full Paper

Antitumor Agents

Exploring the Effect of Polypyridyl Ligands on the Anticancer Activity of Phosphorescent Iridium(III) Complexes: From Proteosynthesis Inhibitors to Photodynamic Therapy Agents

Jitka Pracharova[+],[b] Gloria Vigueras[+],[c] Vojtech Novohradsky,[a] Natalia Cutillas,[c] Christoph Janiak,[d] Hana Kostrhunova,[a] Jana Kasparkova,[a] José Ruiz,*[c] and Viktor Brabec*[a]

Abstract: A series of five kinetically inert bis-cyclometalated Ir^{III} complexes of general formula $[Ir(C\hat{}N)_2(N\hat{}N)][PF_6]$ [C^N = 2-phenyl-1-[4-(trifluoromethyl)benzyl]-1*H*-benzo[*d*]imidazol-κ*N*,*C*; N^N = 1,10-phenanthroline (phen, **1**), dipyrido[3,2-*d*:2′,3′-*f*]quinoxaline (dpq, **2**), dipyrido[3,2-*a*:2′,3′-*c*]phenazine (dppz, **3**), benzo[*i*]dipyrido[3,2-*a*:2′,3′-*c*]phenazine (dppn, **4**), and dipyrido[3,2-*a*:2′,3′-*c*]phenazine-10,11-imidazolone (dppz-izdo, **5**)] were designed and synthesized to explore the effect of the degree of π conjugation of the polypyridyl ligand on their toxicity in cancer cells. We show that less-lipophilic complexes **1** and **2** exhibit the highest toxicity [submicromolar inhibitory concentration (IC_{50}) values] in A2780, HeLa, and MCF-7 cancer cells, and they are markedly more efficient than clinically used platinum drugs. It is noteworthy that the investigated Ir agents display the capability to overcome acquired and inherent resistance to conventional cisplatin (in A2780cisR and MCF-7 cells, respectively). We demonstrate that the Ir complexes, unlike clinically used platinum antitumor drugs, do not kill cells through DNA-damage response. Rather, they kill cells by inhibiting protein translation by targeting preferentially the endoplasmic reticulum. Our findings also reveal that the toxic effect of the Ir complexes can be significantly potentiated by irradiation with visible light (by more than two orders of magnitude). The photopotentiation of the investigated Ir complexes can be attributed to a marked increase (≈10–30-fold) in intracellular reactive oxygen species. Collectively, these data highlight the functional diversity of antitumor metal-based drugs and the usefulness of a mechanism-based rationale for selecting candidate agents that are effective against chemoresistant tumors for further preclinical testing.

Introduction

Chemotherapy is used in most treatment regimens for cancer, and nearly 50% of patients are treated with a platinum-based drug. In spite of their clinical success, traditional Pt^{II}-based drugs for cancer therapy present major drawbacks, such as acquired or intrinsic resistance, limited spectrum of action, and severe side effects in the patient.[1] As an alternative to FDA-approved Pt^{II} complexes, some antitumor organometallic compounds containing a transition metal other than platinum (e.g., ruthenium, iridium, or osmium) were recently identified as promising antitumor agents.[2] Furthermore, it is now generally accepted that simple modifications of organometallic scaffolds dictate target preferences of the drug. Thus, interesting examples of the use of octahedral iridium(III) cyclometalated complexes were recently reported to act as modulators in protein–protein interactions,[3] membrane disruptors,[4] mitochondria-targeted agents,[5] DNA binders,[6] and receptor-targeted compounds.[7] Moreover, cyclometalated Ir^{III} complexes have attracted increasing attention in bioimaging and biosensing ap-

[a] *Dr. V. Novohradsky, Dr. H. Kostrhunova, Prof. Dr. J. Kasparkova, Prof. Dr. V. Brabec*
Institute of Biophysics, Czech Academy of Sciences
Kralovopolska 135, 61265 Brno (Czech Republic)
E-mail: brabec@ibp.cz

[b] *Dr. J. Pracharova[+]*
Department of Biophysics, Centre of the Region Hana for Biotechnological and Agricultural Research, Palacky University
Slechtitelu 27, 783 71 Olomouc (Czech Republic)

[c] *G. Vigueras,[+] Dr. N. Cutillas, Prof. Dr. J. Ruiz*
Departamento de Química Inorgánica
Universidad de Murcia and Institute for Bio-Health Research of Murcia (IMIB-Arrixaca), 30071 Murcia (Spain)
E-mail: jruiz@um.es

[d] *Prof. Dr. C. Janiak*
Institut für Anorganische Chemie und Strukturchemie
Heinrich-Heine-Universität Düsseldorf, Universitätsstr 1
40225 Düsseldorf (Germany)

[+] *These authors contributed equally to this work.*

Supporting information and the ORCID identification numbers for the authors of this article can be found under https://doi.org/10.1002/chem.201705362.

plications[8] because of their rich photophysical properties, which include high quantum yields, large Stokes shifts, long-lived luminescence, good photostability, and cell permeability.

On the other hand, photodynamic therapy (PDT) is a noninvasive medical technique that relies on the use of light to control drug activity along an adaptable time span at a specific space. It is based on the generation of toxic singlet oxygen ($^1O_2$) and/or reactive oxygen species (ROS) through the combination of a nontoxic molecule called a photosensitizer (PS), light, and molecular oxygen ($^3O_2$). $^1O_2$ has a lifetime of approximately 40 ns and then only induces damage in very close proximity to the irradiation site, a key factor in the reduction of the side effects observed for patients subjected to PDT.[9] To date, FDA-approved dye sensitizers for PDT treatment are mainly porphyrinoid compounds.[10] However, their clinical use is limited by the short lifetime of their excited state and the low quantum yield of singlet oxygen production.[11] The vast majority of the metal complexes screened as PSs are octahedral polypyridine Ru^{II} complexes,[12] and the Ru^{II} complex TLD-1433 (a Ru^{II} dyad derived from α-terthienyl appended to imidazo[4,5-*f*][1,10]phenanthroline) has been approved to enter phase Ib clinical trials in Canada (ClinicalTrials.gov Identifier NCT03053635) for the treatment of nonmuscle-invasive bladder cancer.[13] Ir^{III} complexes have risen as potential alternatives to isoelectronic Ru^{II}-based PSs. Unlike most promising Ru^{II} PDT agents, Ir^{III}-based PSs usually contain cyclometalated ligands.[14] The latest examples enable broader tuning of the intrinsic photophysical properties,[15] increased ligand-field stabilization energy, and pronounced decoupling of the triplet metal-to-ligand charge-transfer (^{3}MLCT) excited states with respect to those that are metal centered.[16] Thus, these complexes possess multiple advantages, among which their longer lifetimes (≈microseconds) and ROS generation capabilities under hypoxic conditions stand out.[17]

Herein, we describe a series of luminescent organometallic iridium(III) complexes of the type $[Ir(C^N)_2(N^N)][PF_6]$ (Scheme 1), in which the cyclometalating ligand 2-phenyl-1-[4-(trifluoromethyl)benzyl]-1*H*-benzo[*d*]imidazol remains as the C^N backbone and the diimine ligand is varied {N^N = phen (**1**), dpq (**2**), dppz (**3**), dppn (**4**), and dppz-ido (**5**); phen = 1,10-phenanthroline; dpq = dipyrido[3,2-*d*:2′,3′-*f*]quinoxaline; dppz = dipyrido[3,2-*a*:2′,3′-*c*]phenazine; dppn = benzo[*i*]dipyrido[3,2-*a*:2′,3′-*c*]phenazine; dppz-izdo = dipyrido[3,2-*a*:2′,3′-*c*]phenazine-10,11-imidazolone} with the aim to fine-tune the cytotoxic properties of these types of promising drugs.

Notably, benzimidazole is a widely used pharmacophore,[18] and we previously reported that benzimidazole metal compounds were able to act either as antiangiogenic and/or antitumor agents[7a,19] or amyloid-β aggregation inhibitors.[20] The choice of the trifluoromethylbenzyl group on the nitrogen atom of the benzimidazole supports a higher lipophilic nature of the ligand. The in vitro antiproliferative activities of **1**–**5** were investigated against several human cancer-cell lines both under dark and irradiation conditions. The mechanism of action of **1** and **5** in the dark, which included reactive oxygen species (ROS) elevation and the induction of apoptosis, was additionally estimated by real-time cell electronic sensing in cancer cells. In addition, their activity could be increased by more than two orders of magnitude upon irradiating at $\lambda =$ 420 nm with a markedly (≈10–30-fold) increased intracellular ROS level under irradiation.

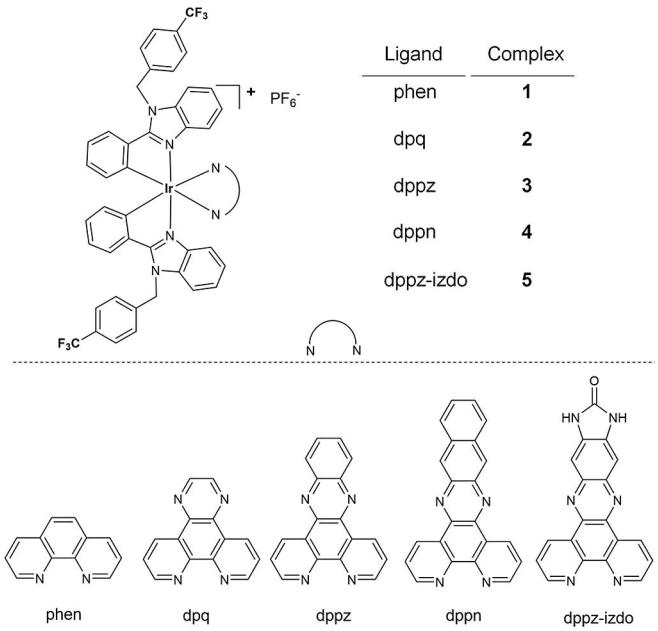

Ligand	Complex
phen	**1**
dpq	**2**
dppz	**3**
dppn	**4**
dppz-izdo	**5**

Scheme 1. Structures of new iridium(III) complexes **1**–**5** for structure–activity relationship studies.

Results and Discussion

Synthesis and characterization of the iridium complexes

A series of five luminescent and substitutionally inert iridium(III) complexes of the type $[Ir(C^N)_2(N^N)][PF_6]$ (Scheme 1) [C^N = 2-phenyl-1-[4-(trifluoromethyl)benzyl]-1*H*-benzo[*d*]imidazol-κ*N*,*C*; N^N = phen (**1**), dpq (**2**), dppz (**3**), dppn (**4**), and dppz-izdo (**5**)] were designed and synthesized to investigate the effect of the nature of the polypyridyl ligands on their antitumor activity. Complexes **1**–**5** were obtained in high yields (65–86%) as their PF_6^- salts by the reaction of the cyclometalated Ir^{III} dimer with the corresponding N^N ligand in a 1:2 molar ratio. All complexes were characterized by ^{1}H NMR and ^{13}C NMR spectroscopy, positive-ion ESI-HRMS, and UV/Vis spectroscopy. All compounds were shown to be at least 96% pure by both reverse-phase (RP) HPLC in DMSO (Figure S7 in the Supporting Information) and elemental analysis. The positive-ion ESI mass spectra displayed the $[M-PF_6]^+$ signals with the expected isotopic distribution pattern. The stability of the complexes in DMSO was studied by ^{1}H NMR spectroscopy, and no free ligands were detected after 24 h at room temperature (see Figure S6 for **5**). The stability of the complexes was also confirmed after 24 h in Roswell Park Memorial Institute (RPMI) culture medium by HPLC upon dissolving the compounds in 5% DMSO (see Figure S8 for **1**–**5**). The photostability in H_2O/DMSO solution was ascertained for **3** by UV/Vis spectroscopy after irradiation at $\lambda = 420$ nm for 15 min, and no changes in

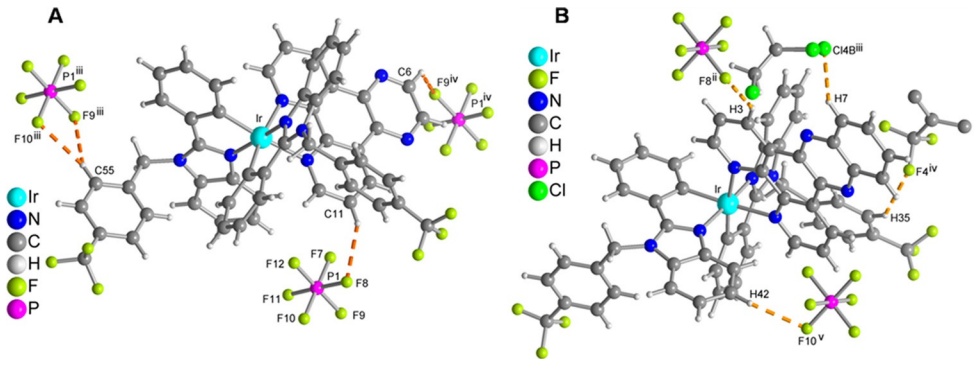

Figure 1. Molecular structures with hydrogen-bonding schemes for: A) **2**, showing the iridium complex cation and three surrounding PF_6 anions in the crystal structure (CH_2Cl_2 solvent molecules of crystallization are omitted for clarity), and B) **3**, showing the iridium complex cation and two surrounding PF_6 anions, a trifluoromethylphenyl fragment from an adjacent cation, and a $C_2H_4Cl_2$ solvent molecule in the crystal structure. Details of hydrogen bonds including the symmetry transformations are given in Table S8.

the spectra before and after light exposure (Figure S15) were observed.

Single crystals suitable for X-ray diffraction analysis were obtained by slow diffusion of hexane into saturated solutions of **2** and **3** in CH_2Cl_2 and 1,2-dichloroethane, respectively. Their structures and part of the hydrogen-bonding schemes are shown in Figure 1. Crystallographic data are given in Tables S3–S8, and selected bond lengths and angles are listed in Table S9. The Ir atoms have a pseudo-octahedral coordination geometry, and the largest deviation is represented by the bite angle (from 77.6 to 77.98°) of the polypyridine ancillary ligand. The two Ir–C bonds are in a mutual *cis* arrangement, and their high *trans* influence results in Ir–N bond lengths that are slightly shorter in the C^N ligands than in the N^N ligands. These findings are commonly observed for related cyclometalated Ir^{III} complexes.[5a] The singly positive complex cation of **2** crystallized with one PF_6 anion and approximately 1.75 methylene chloride solvent molecules. The complex cation of **3** crystallized with one PF_6 anion and approximately 2.375 1,2-dichloroethane and one hexane solvent molecules per formula unit, exhibiting disorder of the solvent molecules within the solvent-occupied voids between the complex molecules. Besides the important cation–anion Coulomb interactions, the packing in the structures of **2** and **3** is organized (according to analysis by PLATON[21]) by intermolecular C–H···F[22] (Tables S10 and S13), C–H···Cl contacts (only for **3**), C–H···π interactions[23] (Tables S11 and S14, Figures S17 and S20), and π–π interactions[24] (only one for **2** and a few for **3**; Schemes S2 and S8, Tables S12 and S15). The π–π interactions between the dipyridophenazine ligands of **3** lead to pairwise arrangement of two symmetry-related molecules (see Figure S21).

The UV/Vis absorption spectra were recorded for complexes **1**–**5** in Tris buffer (Tris·HCl/DMSO = 99:1), CH_3CN, and H_2O/DMSO (99:1) solutions at room temperature. They are characterized by multiple bands (Figure 2A for **1**–**5** in H_2O/DMSO, and Figures S9 and S10), and the most significant absorption data are collected in Table S2. All complexes show high-intensity, high-energy bands at $\lambda < 350$ nm that can be attributed to spin-allowed ligand-centered (^{1}LC) π–π* transitions for the cyclometalated (C^N) and ancillary (N^N) ligands. The relatively low-energy bands ($\lambda > 350$ nm) can be assigned to mixed singlet and triplet metal-to-ligand charge-transfer (spin-allowed singlet-to-singlet ^{1}MLCT and spin-forbidden singlet-to-triplet ^{3}MLCT) and ligand-to-ligand charge-transfer (LLCT) transitions.[25] Upon excitation at $\lambda = 380$ nm (for **1**–**4**) or $\lambda = 405$ nm (for **5**), the new iridium complexes exhibit long-lived yellow-to-orange phosphorescence (Figures 2B and S11), and the emission is slightly sensitive to the nature of the solvent (Table S2).

The emission lifetimes of **1**–**5** in H_2O/DMSO in the 140–279 ns range (Table 1) are consistent with excited states of triplet parentage.[26] A decrease in the emission intensity (Figure 2B) is observed upon increasing the length of the poly-

Table 1. Excitation wavelengths (λ_{ex}), emission wavelengths (λ_{em}), emission lifetimes (τ_{em}), and quantum yields (Φ_{em}) of **1**–**5** in H_2O/DMSO (99:1).

Compd	λ_{ex}[a] [nm]	λ_{em} [nm]	τ_{em}[b] [ns]	Φ_{em}[c] [%]
1	381	557	269	22.3
2	381	582	279	10.5
3	380	595	140	1.5
4	380	566	270	< 1
5	405	580	148	< 1

[a] λ_{ex} maxima. [b] Emission lifetime measured in aerated solutions. [c] Emission quantum yields measured in deaerated H_2O/DMSO solution.

pyridyl N^N ligand so that the quantum yields of **1**–**5** in H_2O/DMSO range from < 1 (for **4**) to 22.3% (for **1**). As no change in emission intensity is observed between aerated and deaerated solutions (Figure 2C), the emission intensity decrease is ascribed to the luminescence aggregation-caused quenching (ACQ) effect.[27] ^{1}H NMR spectroscopy was used to probe the extent of aggregation for the complexes. An upfield shift in some aromatic resonances of the N^N ligand is observed in the spectrum of **4** upon increasing the concentration (Figures S12B and at different compositions of mixtures of [D_6]DMSO and D_2O (Figure S13 for **4** and **5**). This effect can be attributed to favorable π–π stacking, which is well known to lead to the formation of dimers in solution or even higher order aggregates.[28] In fact, an increase in the water content up to 70%

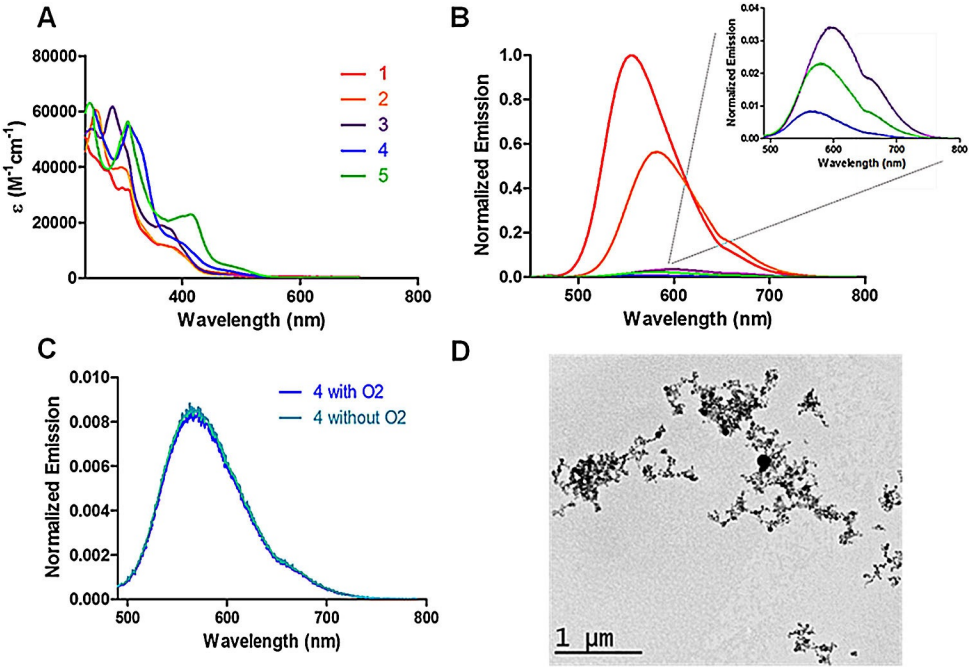

Figure 2. a) UV/Vis absorption spectra, and b) emission spectra of complexes **1**–**5** in H_2O/DMSO (99:1) at room temperature. The excitation wavelength was 405 nm. c) Emission spectra of **4** in aerated and deaerated H_2O/DMSO solution; $\lambda_{exc} = 405$ nm. d) TEM image of the aggregates prepared from **4** in H_2O/DMSO.

gives broad signals that lead to the virtual disappearance of the resonances in the ^{1}H NMR spectra of **4** and **5** (Figure S13). This behavior is not observed for complex **1**, for which the degree of π conjugation of the polypyridyl ligand is lower (Figure S12 A). The aggregation of **4** and **5** was verified by transmission electron microscopy (TEM), which revealed (Figures 2 D and S14) spherical and elongated aggregates in H_2O/DMSO (10 μM), respectively.

Cytotoxicity towards human cancer cells

The cytotoxic effects of the Ir compounds against four human tumor cell lines (ovarian A2780, cisplatin-resistant ovarian A2780cisR, cervix HeLa, and breast MCF-7 cells) were evaluated by using the standard 3-(4,5-dimethylthiazol-2-yl)-2,5-diphenyltetrazolium bromide (MTT) assay. For comparative purposes, the cytotoxicity of the clinically used metallodrug cisplatin was also evaluated under the same experimental conditions. As indicated in Table 2 and Figure S30, the investigated Ir complexes were toxic in all cancer cell lines tested.

The cytotoxic potency of the new iridium complexes decreased in the order **1** ≈ **2** > **3** > **5** > **4**, that is, roughly with an increase in both the largeness of the polypyridyl ligand and the lipophilicity of the complex (roughly determined by the retention times in RP-HPLC analyses; Figure S7, Table 3, and see below). Interestingly, all investigated Ir complexes were able to overcome acquired resistance to cisplatin and were at least as cytotoxic in cisplatin-resistant A2780cisR cells as in the wild-type A2780 line. The resistance factor, defined as the ratio of the inhibitory concentration (IC_{50}) values in resistant (A2780cisR) and cisplatin-sensitive parent cells (A2780), was in the range of 0.34 to 1.02 for the Ir complexes, whereas it was markedly higher for cisplatin (2.89). Moreover, the investigated Ir complexes (except **4**) were also more toxic than cisplatin in breast MCF-7 cells, which are naturally resistant towards cisplatin. These results suggest that the mechanism underlying the biological action of the Ir complexes should be different from

Table 2. Cytotoxicity obtained for complexes **1**–**5** and cisplatin (cisPt).[a]

Compd	IC_{50} [μM]		RF	IC_{50} [μM]			SI
	A2780	A2780cisR		HeLa	MCF-7	MCF-10A	
cisPt	5.4 ± 0.4	15.5 ± 0.4	2.9	14.0 ± 0.9	16.6 ± 0.7	20 ± 2	1.2
1	0.63 ± 0.03	0.38 ± 0.09	0.6	1.8 ± 0.1	0.7 ± 0.1	2.6 ± 0.3	3.7
2	1.1 ± 0.1	0.37 ± 0.09	0.3	0.9 ± 0.2	0.5 ± 0.1	3.2 ± 0.2	6.4
3	2.9 ± 0.6	2.80 ± 0.01	0.9	6.1 ± 0.3	6.3 ± 0.8	9.9 ± 0.8	1.6
4	20 ± 3	20 ± 2	1.0	> 25	23 ± 2	40 ± 4	1.7
5	4.7 ± 0.6	3.4 ± 0.5	0.7	23 ± 3	11 ± 3	41 ± 3	3.7

[a] The results are expressed as mean ± SD of three independent experiments, each of them made in quadruplicate. Resistance factor (RF) is defined as IC_{50}(resistant cells)/IC_{50}(sensitive cells). Selectivity index (SI) is defined as IC_{50}(nonmalignant MCF-10A cells)/IC_{50}(cancer MCF-7 cells).

Table 3. Retention times (t_R) by RP-HPLC and cellular accumulation of cisplatin and the investigated Ir complexes in HeLa cells.[a]

Compd	t_R [min]	Uptake[a] [pmol per 10^6 cells]	
		5 h	24 h
cisplatin	–	22.7 ± 0.7	110 ± 10
1	17.1	34 ± 4	61.0 ± 0.9
2	17.4	105 ± 11	219 ± 9
3	18.5	305 ± 5	536 ± 12
4	19.1	275 ± 11	461 ± 55
5	17.2	246.0 ± 13	406 ± 12

[a] Cellular uptake of the investigated metal compounds (10 μM) into HeLa cells after 5 or 24 h. The results are expressed as the mean ± SD of three independent experiments.

that of clinically used cisplatin and its direct derivatives, which allows the Ir complexes to overcome the resistance mechanisms operating in the case of conventional platinum anticancer drugs. Last, but not least, the results shown in Table 2 show that the investigated iridium complexes are less cytotoxic in noncancerous breast cells, MCF-10A, and exhibit higher selectivity for breast cancer cells, MCF-7, than the conventional platinum anticancer drug cisplatin.

DNA interactions in cell-free media

A number of antitumor metal-based drugs (e.g., several platinum[29] and ruthenium[30] complexes) have demonstrated a high ability to interact and damage nuclear DNA, which is considered their important pharmacological target. In addition, some cyclometalated iridium(III) complexes containing extended conjugated aromatic ligands capable of DNA intercalation have shown nuclear or perinuclear accumulation.[31] In this context, we expected that the new Ir complexes investigated in this study might be directed, after their accumulation in cells, to the cell nucleus, at which they would interact with nuclear DNA.

Therefore, we performed experiments to demonstrate that the new investigated Ir complexes were able to interact with DNA. We investigated reactions of complexes **1**–**5** with naked mammalian DNA in cell-free media to elucidate whether the presence of DNA intercalating ligands in the investigated Ir complexes promoted their interaction with DNA. For this purpose, we employed several biochemical and biophysical methods. The individual experiments and the results obtained are described in the Supporting Information (Figures S22–S29 and Tables S16 and S17). In summary, the results of these experiments reveal that **1** and **2** do not interact with double-helical DNA in cell-free media, whereas **4** and **5** (and also **3** to a markedly lower extent) do interact with DNA. However, their DNA binding mode comprised a groove binding rather than the expected intercalation. Collectively, these data show that the DNA binding affinity of the investigated Ir complexes increases with the largeness of their phenanthroline-based ligands. Hence, the DNA binding affinity of the investigated Ir complexes inversely correlates with their cytotoxicity, so that DNA binding does not seem to play a decisive role in the mechanism of biological action of these compounds.

Cellular accumulation

The biological action of metal-based drugs is strongly dependent on their abilities to cross cellular membranes and enter the cells. Despite the fact that in cell-free media the compound binds and influences its target(s), the resulting cytotoxicity can be reduced significantly by a low accumulation in cells. Therefore, the intracellular content of Ir from the investigated Ir complexes was determined in human HeLa cancer cells treated with equimolar (10 μM) concentrations of complexes **1**–**5** for 5 and 24 h. The iridium (or platinum in the case of cisplatin) contents in the samples were determined by inductively coupled plasma (ICP) MS. It was verified that no marked increase in dead cells was observed in comparison with the control, untreated cells. The viability of these cells was approximately 85–97%. Both live and dead cells were harvested and included in the experiment. Thus, the viability of the cells in the cellular accumulation experiments was reduced only negligibly so that it could not considerably affect the amount of iridium which accumulated in cells under the conditions of the experiments summarized in Table 3.

As indicated in Table 3, the amount of iridium that accumulated in cells after 5 or 24 h of treatment increased in the order $\mathbf{1} < \mathbf{2} < \mathbf{3} \approx \mathbf{4} \approx \mathbf{5}$. Although most lipophilic complexes **3** and **4** showed the highest accumulation, the correlation does not work for **5**. The effect of the N,N-chelate on drug lipophilicity was studied by comparing their RP-HPLC retention times (t_R) on a C18 column (Table 3 and Figure S7; this is considered a reliable method to estimate the relative hydrophobicities, as the RP-HPLC behavior of a compound depends on its hydrophobic interactions with the nonpolar stationary phase: more lipophilic complexes should have larger retention times[19b,32]). This correlation suggests a role of passive diffusion in the cellular uptake of these compounds (except for **5**). Interestingly, most active **1** showed the lowest accumulation in cells, whereas much less active **4** and **5** showed an accumulation almost one order of magnitude higher. Thus, the cytotoxicities of the investigated Ir compounds do not simply reflect their ability to accumulate in cells.

Real-time cell electronic sensing

Impedance-based time-dependent cell-response profiling was used as the predictive method for the mechanism of biological action of the investigated Ir compounds. It was previously shown that profiles of time-dependent cell-response curves could be used to partially identify the mechanism of action of small molecules.[33] The time-dependent cell-response profiles (TCRPs) of **1** and **5** are characterized by an initial increase in the cell index (CI) above the level of the CI for the control, followed by a peak with a width that is inversely proportional to the concentration of the investigated compound applied to the cells (shown in Figure 3 for HeLa and A2780 cells treated

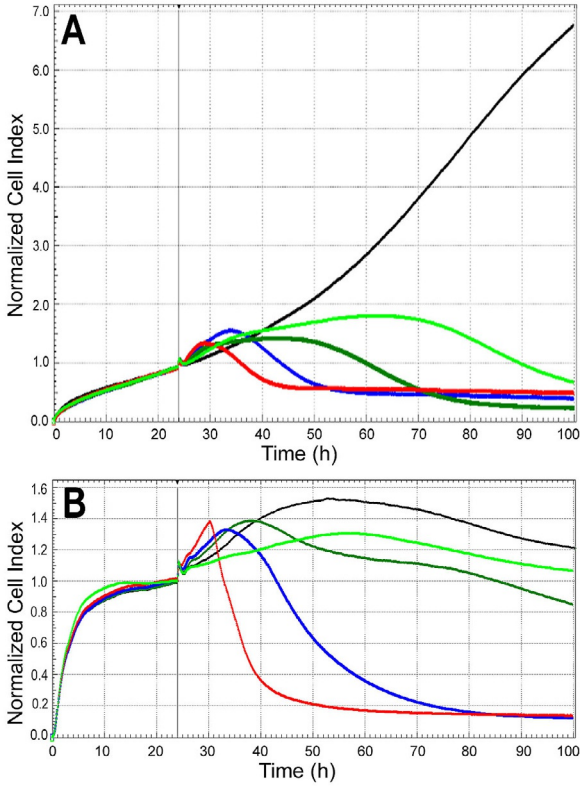

Figure 3. TCRPs of: a) A2780, and b) HeLa cells treated with increasing concentrations of **1**. Curves: untreated control (black line) and **1** at concentrations of 1 μM (light green), 3 μM (dark green), 10 μM (blue), and 20 μM (red). Data were normalized to the time of the treatment and are expressed as the normalized cell index. Curve profiles of **5** were found to be the same as those of **1** at a concentration approximately 5 times higher. Thus, only the results for **1** are shown.

with **1**). The slope of the CI decline is directly proportional to the treated concentration.

The obtained profiles (Figure 3) were compared to those of a library of compounds that were clustered into groups on the basis of the similarities of their mechanism of action.

The TCRPs of **1** and **5** were the same as those of the group of compounds affecting protein synthesis; moreover, complete match with anisomycin was found.[33a] This model compound inhibits peptidyl transferase, which is an integral part of the large subunit of ribosomes, and catalyzes peptide-bond formation in the elongation step of translation during protein biosynthesis.[34] Altogether, the TCRPs obtained for the investigated Ir complexes (Figure 3) are consistent with the view and support the hypothesis that a possible mechanism of action of the Ir complexes involves inhibition of protein translation.

To support further the thesis that a possible mechanism of action of the investigated Ir complexes involved inhibition of protein translation, the incorporation of [^{35}S]methionine ([^{35}S]-Met) was detected as a measure of translation activity of the cells in the presence of the investigated Ir complexes. In these experiments, we intentionally used low concentrations of **1** or **5** and a short incubation time (1 h) to secure cell viability so as to detect mainly the upstream effects of the Ir complexes. HeLa cells were further incubated with [^{35}S]-Met for 2 h to

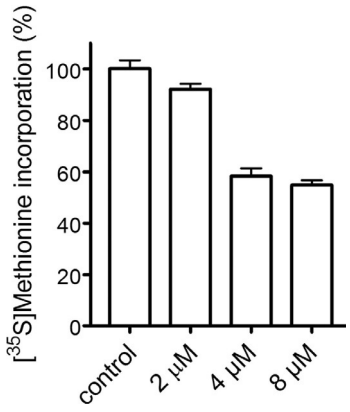

Figure 4. Effect of **1** on translation in HeLa cells as a measure of the incorporation of [^{35}S]methionone. The radioactivity of the control, untreated cells was taken as 100%. Cells were treated with **1** at the indicated concentrations for 1 h. Bars represent mean ± SD from two independent measurements.

allow their incorporation into the newly synthesized proteins. The Ir complexes significantly decreased protein synthesis (shown for **1** in Figure 4).

Cellular localization by fluorescence confocal microscopy

Fluorescence cell microscopy was used to ascertain the cellular distribution of the investigated Ir compounds. For this study, we selected two representative compounds of the five investigated Ir complexes, namely, **1**, which does not interact with DNA (and that exhibits a high quantum yield value in cell-free media), and **5**, which binds DNA in vitro with the highest affinity. It is noteworthy that **5** showed a luminescence switch-on effect within cancer cells, despite having a luminescence aggregation-caused quenching effect in H_2O/DMSO solvent.

As indicated in Figure 5 A, no significant difference in the localization of the luminescence from either compound in HeLa cells was observed. The luminescence from both complexes was localized preferentially out of the cell nucleus, and the majority of the luminescence was associated with the cytoplasm. Hence, these results further support the thesis that DNA interaction is not a major factor contributing to the biological effects of the investigated Ir complexes.

On the basis of the results of real-time cell electronic sensing (Figure 3) and the fact that DNA is a very unlikely target for the investigated Ir compounds, we also performed a co-localization study, which may suggest the intracellular target organelle. Moreover, to study whether the presence of DNA interacting ligands in the investigated Ir compounds could affect their localization in living cells, the fluorescence properties of these complexes were utilized.

The fluorescence signal coming from the investigated Ir compounds almost completely matched the fluorescence coming from endoplasmic reticulum (ER)-Tracker marked organelles (Figure 5). Co-localization of **1** and **5** with the ER was also analyzed by using the Pearson's correlation coefficient (PCC).[35] The PCCs above the threshold were 0.43 ± 0.03 and 0.60 ± 0.02 for **1** and **5**, respectively. The calculated PCCs con-

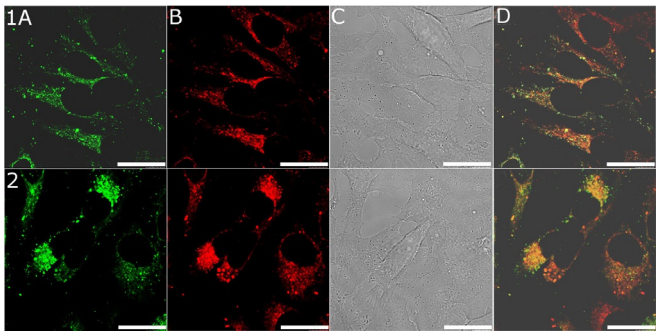

Figure 5. Co-localization studies of **1** and **5** in HeLa cells. HeLa cells were treated with 5 μM of **1** (1) and **5** (2) for 2 h and were co-stained with ER-Tracker. Channels: a) fluorescence signal from the tested compounds, b) ER-Tracker fluorescence, c) bright field, d) overlay of the fluorescence channels. Samples were sequentially scanned with a confocal laser scanning microscope, and the scale bars are 25 μm.

firmed a high level of co-localization with the ER for both compounds. These results underscore the ability of the investigated Ir complexes to target the ER preferentially.

Cell-death detection

Cytotoxicity testing (Table 2) revealed that complexes **1**–**5** were able to induce cell death. Many metal-based compounds capable of killing cancer cells act by triggering cellular processes leading to apoptosis.[1a,36] However, cytotoxic compounds may also kill cells through nonapoptotic cell-death pathways such as necrosis.[37] To distinguish whether the cells treated with the investigated Ir complexes underwent apoptosis or necrosis, DNA fragmentation induced by various concentrations of **1** and **5** was quantified by a specific ELISA colorimetric kit. This analysis allows relative amounts of cytoplasmic histone-associated DNA fragments (mono- and oligonucleosomes) to be measured after they are produced during the apoptotic process or if these fragments are released from necrotic cells. Figure 6 shows DNA fragmentation induced by equitoxic concentrations of both **1** and **5** in HeLa cells as a result of cell-death processes. These results demonstrate that treatment of cancer cells with both Ir complexes led primarily to apoptotic events.

A number of cytotoxic metal-based agents including clinically used platinum drugs induce apoptosis in cancer cells primarily through targeting and damaging nuclear DNA.[1a] Even though DNA interaction is not very likely an important factor contributing to the biological effects of the investigated Ir complexes (see above), in vitro mechanistic studies confirmed that these Ir complexes also displayed an apoptotic mechanism of action (rather than necrosis) (Figure 6). Hence, the investigated Ir complexes appear to induce apoptosis in a manner different from that of conventional antitumor metal-based drugs.

Photopotentiation by visible light

Some iridium-based complexes have been shown[2a,38] to be sensitive to light irradiation. Thus, the effect of visible light on

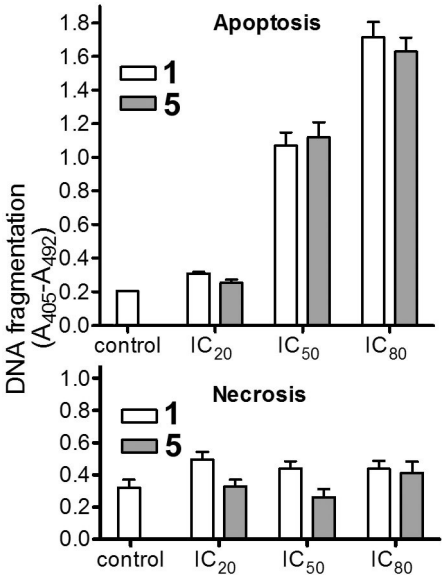

Figure 6. Detection of apoptosis and necrosis in HeLa cells treated with equitoxic (IC_{20}, IC_{50}, and IC_{80}) concentrations of **1** and **5** for 24 h. Data show mean ± SD from two independent experiments, each of them made in duplicate.

the cytotoxic properties of the investigated Ir complexes was also tested. HeLa cells were treated with the Ir complexes in Earle's balanced salt solution (EBSS) for 1 h in the dark to give the compounds time to enter the cells, and subsequently, the cells were irradiated with blue light (λ_{max} = 420 nm) for 1 h. After irradiation, the cells were washed and incubated in complete Dulbecco's modified Eagle medium (DMEM) (without Ir complex) for another 70 h (recovery time). Then, the viability of the cells was assessed by the MTT test, as described in the Experimental Section.

As indicated in Table 4, the toxic effects of all the investigated Ir complexes in HeLa cells were significantly potentiated by irradiation with visible light. The phototoxicities of all the compounds were elevated by more than two orders of magnitude compared to the sham-irradiated samples.

Table 4. Phototoxicity of the investigated Ir complexes in HeLa cells.[a]

Compd	IC_{50} [μM]	
	SHAM	420 nm
1	11.5 ± 0.2	0.044 ± 0.006
2	10.36 ± 0.06	0.103 ± 0.005
3	> 100	0.866 ± 0.009
4	> 50	0.58 ± 0.01
5	> 50	0.35 ± 001

[a] Results are expressed as mean ± SD of three independent experiments, each of them made in quadruplicate.

Determination of intracellular reactive oxygen species (ROS)

It was already shown[14a,38,39] that upon irradiation iridium complexes could significantly increase intracellular ROS levels.

Therefore, intracellular ROS were quantified to determine the oxidative stress in cells after treatment with **1** or **5** in the dark and under $\lambda = 420$ nm light irradiation. A method developed by Robinson et al.[40] was used. This method was designed to provide a highly sensitive, quantifiable, real-time assessment of ROS production.[33b] To evaluate ROS formation, HeLa cells untreated or treated with **1** or **5** in the dark or under irradiation conditions ($\lambda_{max} = 420$ nm) were incubated with 10 μM 2′,7′-dichlorodihydrofluorescein diacetate (DCFH-DA) for 30 min in the dark. DCFH-DA, after cleavage by cellular esterases, is oxidized by ROS to yield a fluorescent product, the fluorescence of which was measured. The data demonstrating the generation of ROS in HeLa cells induced by various concentrations of **1** or **5** are plotted in Figure 7.

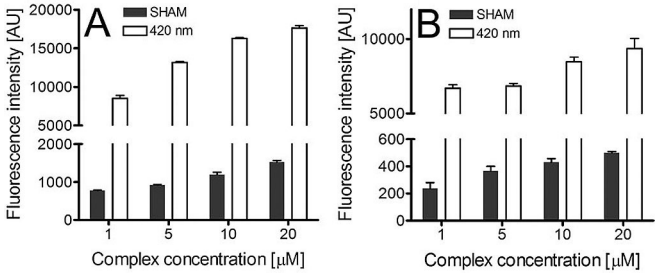

Figure 7. Generation of ROS in HeLa cells induced by various concentrations of **1** (panel a) or **5** (panel b). The values shown in this figure represent the fluorescence intensity in arbitrary units (AU) obtained for various concentrations of the investigated Ir complexes, from which the fluorescence intensity obtained for the untreated control cells was subtracted. The fluorescence intensities yielded by the untreated cells in the dark or under irradiation conditions were (333 ± 57) or (438 ± 57) AU, respectively. Data represent mean ± SD from three independent measurements.

Treatment of HeLa cells with **1** in the dark resulted in a concentration-dependent increase in fluorescence (Figure 7 A, black bars), which indicated the production of ROS. Importantly, the fluorescence was markedly (11–14-fold) increased if the treated cells were irradiated before ROS were detected (Figure 7 A, white bars). This implies that the level of intracellular ROS induced by **1** could be markedly elevated by irradiation with visible (blue) light. Complex **5** showed effects that were qualitatively similar (i.e., 18–28-fold increase in intracellular ROS level upon irradiation, Figure 7B), but altogether, it was less effective in inducing ROS than **1**, which likely reflects its lower cytotoxicity under both dark and irradiation conditions.

Conclusions

Herein, we reported the synthesis and characterization of a series of Ir^{III} complexes of type $[Ir(C^N)_2(N^N)][PF_6]$ with 2-phenyl-1-[4-(trifluoromethyl)benzyl]-1*H*-benzo[*d*]imidazole cyclometalating ligands and various polypyridyl ancillary ligands. The aim was to develop new, preclinically interesting chemotherapeutic agents with a novel mechanism of action.

First, we discovered that the complexes exhibited different photophysical properties depending on the length and degree of π-conjugation of the N^N ligand; the largest exhibited a luminescence aggregation-caused quenching effect in cell-free media. Their cytotoxicity was studied in several cancer cell lines. Less lipophilic complexes **1** and **2** (which displayed the lowest level of cellular accumulation) exhibited the highest toxicities (sub-micromolar IC_{50} values) in A2780, HeLa, and MCF-7 cancer cells, and they were markedly more efficient than clinically used platinum drugs. In contrast, the cytotoxicities of more lipophilic **4** and **5** were considerably diminished (IC_{50} values were ≈4–55-fold higher). It is noteworthy that the investigated Ir agents displayed the capability to overcome acquired and inherent resistance to conventional cisplatin (in A2780cisR and MCF-7 cells, respectively) and were more selective for breast cancer cells than healthy breast cells. In our quest to investigate the mechanism of cytotoxicity of the investigated Ir complexes, we first examined whether these Ir compounds were capable of interacting and damaging DNA. These investigations were substantiated by the fact that some cyclometalated iridium(III) complexes containing extended conjugated aromatic ligands capable of DNA intercalation accumulated in the cell nucleus and interacted with nuclear DNA. We demonstrated by using several biochemical and biophysical methods that DNA binding affinity of the investigated Ir complexes inversely correlated with their cytotoxicity so that DNA binding did not seem to play a key role in the mechanism of biological action of these compounds. In addition, we also demonstrated that the cytotoxicity of the Ir complexes did not reflect their cellular accumulation and that they preferentially targeted the endoplasmic reticulum. The time-dependent cell-response profiles and estimations of the incorporation of [^{35}S]methionine as a measure of translation activity of the cells in the presence of the investigated Ir complexes suggested that a possible mechanism of action involved inhibition of protein translation. Thus, we found that the investigated Ir complexes induced apoptosis similarly to other antitumor metal-based drugs but in a different manner. With this in mind, it is noteworthy to mention that very recently a study was published[41] in which it was demonstrated that unexpectedly the antitumor platinum complex oxaliplatin killed cells by inducing ribosome biogenesis stress and not by eliciting a DNA-damage response, as believed up to recently. Similarly, we demonstrated in our recent work[19d] that novel kinetically inert C,N-cyclometalated Ru^{II} complexes also interfered with protein synthesis with a markedly higher potency than conventional inhibitors of DNA translation. Interestingly, the latter mechanism has not hitherto been described for other cytotoxic Ru compounds.

Our examinations also indicated that the toxic effect of all investigated Ir complexes in HeLa cells was significantly elevated (by more than two orders of magnitude) by irradiation with visible light ($\lambda = 420$ nm). This photopotentiation of the investigated Ir complexes was attributed to a marked increase (≈10–30-fold) in intracellular reactive oxygen species. To the best of our knowledge, the Ir complexes investigated in this study represent the first iridium complexes to induce cancer-cell death by inhibition of translation targeting the endoplasmic reticulum, the activity of which could be markedly photopotentiated. Thus, this class of iridium complexes is preclinically appealing, as they offer the potential for non-cross-resistance with ex-

isting chemotherapies by benefiting from the unique mechanism of action and the use of light to control their activity at a desired time and place by visible light.

Experimental Section

General methods and materials

The C, H, and N analyses were performed with a Carlo Erba model EA 1108 microanalyzer. ^{1}H NMR and ^{13}C NMR spectra were recorded with a Bruker AC 300E, Bruker AV 400, or Bruker AV 600 NMR spectrometer. Chemical shifts are cited relative to $SiMe_4$ (^{1}H and ^{13}C, external). ESI mass (positive mode) analyses were performed with an HPLC/MS TOF 6220. The isotopic distribution of the heaviest set of signals matched very closely to that calculated for the formulation of the complex cation in every case. All synthetic manipulations were performed under a nitrogen atmosphere by using standard Schlenk techniques. Solvents were dried by the usual methods. 1,10-Phenanthroline was obtained from Sigma–Aldrich (Madrid, Spain), and iridium chloride was obtained from Johnson Matthey. Deuterated solvents were obtained from Euriso-top. The purity of all biologically evaluated molecules, based on elemental analysis and HPLC, was >96%. Cisplatin (purity ≥99.9% based on elemental and ICP trace analysis) was from Sigma (Prague, Czech Republic). Ir complexes were always freshly prepared in DMSO before use. 3-(4,5-Dimethylthiazol-2-yl)-2,5-diphenyltetrazolium bromide (MTT) was from Calbiochem (Darmstadt, Germany). RPMI 1640 medium, DMEM, fetal bovine serum (FBS), and trypsin/ethylenediaminetetraacetic acid (EDTA) were from PAA (Pasching, Austria). Gentamycin was from Serva (Heidelberg, Germany).

Synthesis

Ligands: The quinoxaline and phenazine ligands (dpq, dppz, dppn,[42] and dppz-izdo[43]) were synthesized through Schiff-base condensation of 1,10-phenantroline-5,6-dione with ethylenediamine, *o*-phenylenediamine, 2,3-diaminonaphthalene, and 5,6-diaminobenzimidazolone-2 as previously reported. The cyclometalating proligand 2-phenyl-1-[4-(trifluoromethyl)benzyl]-1*H*-benzo[*d*]imidazole was synthesized as previously reported.[19c]

Dimer complex [(C^N)$_2$Ir(μ-Cl)]$_2$:[19c] 2-Phenyl-1-[4-(trifluoromethyl)benzyl]-1*H*-benzo[*d*]imidazole (2.2 mmol) and iridium(III) chloride (1 mmol) were dissolved in 2-ethoxyethanol/deionized H_2O (3:1) in a round-bottomed flask. The mixture was stirred at 110 °C for 24 h under a nitrogen atmosphere. The mixture was cooled to room temperature, and the resultant solid was collected by filtration. The solid was washed with water and ethanol.

Complexes 1–5: The cyclometalated iridium(III) chloro-bridged dimer (1.0 mmol) and the respective N^N ligand (2.1 mmol) were dissolved in dichloromethane/methanol (2:3, *v/v*) in a round-bottomed flask. The mixture was stirred at 58 °C for 24 h under a nitrogen atmosphere. After cooling the solution to room temperature, an excess amount of KPF_6 (2.5 mmol) was added, and the mixture was stirred for 30 min. The solvent was removed under reduced pressure, and the product was washed with water. The product was recrystallized from dichloromethane and ether.

Compound 1: Yellow solid (65%); ^{1}H NMR (400 MHz, [D$_6$]DMSO): δ=8.95 (dd, J=8.4, 1.2 Hz, 2H), 8.43 (dd, J=5.2, 1.2 Hz, 2H), 8.37 (s, 1H), 7.72 (m, 8H), 7.29 (d, J=8.0 Hz, 4H), 7.17 (t, J=8.4 Hz, 2H), 6.95 (m, 2H), 6.90 (m, 2H), 6.78 (t, J=7.6 Hz, 2H), 6.40 (dd, J=7.6, 1.2 Hz, 2H), 6.29 (br s, NCH_2Ar, 4H), 5.31 ppm (d, J=8.4 Hz, 2H); ^{13}C NMR (50 MHz, [D$_6$]DMSO): δ=164.18, 153.10, 152.72, 148.60, 142.19, 140.31, 139.63, 136.54, 134.82, 134.38, 131.91, 129.86, 129.63, 129.35, 128.03, 127.31, 127.08, 125.70, 125.11, 123.75, 114.14, 113.30, 48.26 ppm; MS (ESI+, CH_2Cl_2): *m/z* 1051.2519 [M−PF_6]$^+$; elemental analysis calcd (%) for $C_{54}H_{36}F_{12}IrN_6P$: C 53.16, H 2.97, N 6.89; found: C 53.04, H 2.91, N 6.81.

Compound 2: Bright-orange solid (83%); ^{1}H NMR (300 MHz, CD_3CN): δ=9.70 (dd, J=8.4, 1.5 Hz, 2H), 9.21 (s, 2H), 8.60 (dd, J=5.1, 3.6 Hz, 2H), 8.07 (dd, J=8.1, 5.1 Hz, 2H), 7.72 (d, J=7.2 Hz, 2H), 7.67 (d, J=8.1 Hz, 4H), 7.50 (d, J=8.4 Hz, 2H), 7.31 (d, J=8.1 Hz, 4H), 7.18 (td, J=7.2, 0.9 Hz, 2H), 6.98 (td, J=7.5, 1.5 Hz, 2H), 6.90 (td, J=7.5, 1.2 Hz, 2H), 6.79 (td, J=8.4, 1.2 Hz, 2H), 6.53 (dd, J=7.5, 0.9 Hz, 2H), 6.10 (br s, NCH_2Ar, 4H), 5.62 ppm (d, J=8.1 Hz, 2H); ^{13}C NMR (75.4 MHz, CD_3CN): δ=164.35, 154.21, 152.38, 150.32, 147.74, 141.23, 140.67, 139.82, 136.42, 136.04, 134.86, 134.48, 131.55, 131.01, 128.78, 127.73, 126.94, 126.69, 125.52, 124.90, 123.62, 114.96, 112.04, 48.49 ppm; MS (ESI+, CH_3CN): *m/z* 1127.2638 [M−PF_6]$^+$; elemental analysis calcd (%) for $C_{56}H_{36}F_{12}IrN_8P$: C 52.87, H 2.85, N 8.81; found: C 52.65, H 2.65, N 8.47.

Compound 3: Orange-ish-brown solid (79%); ^{1}H NMR (400 MHz, CD_3CN): δ=9.81 (dd, J=8.4, 1.2 Hz, 2H), 8.60 (dd, J=5.2, 1.6 Hz, 2H), 8.46 (dd, J=6.8, 3.6 Hz, 2H), 8.12 (dd, J=6.8, 3.6 Hz, 2H), 8.07 (dd, J=8.0, 2.8 Hz, 2H), 7.73 (d, J=7.6 Hz, 2H), 7.68 (d, J=8.0 Hz, 4H), 7.51 (d, J=8.0 Hz, 2H), 7.33 (d, J=8.4 Hz, 4H), 7.18 (t, J=8 Hz, 2H), 6.99 (t, J=6.8 Hz, 2H), 6.91 (t, J=7.2 Hz, 2H), 6.82 (t, J=8 Hz, 2H), 6.53 (d, J=7.2 Hz, 2H), 6.12 (br s, NCH_2Ar, 4H), 5.73 ppm (d, J=8.0 Hz, 2H); ^{13}C NMR (100 MHz, CD_3CN): δ=164.28, 154.16, 152.27, 151.36, 143.60, 141.12, 140.79, 139.76, 136.36, 136.07, 134.75, 134.35, 133.34, 131.48, 130.45, 129.01, 127.64, 126.83, 126.61, 125.48, 124.83, 123.55, 114.97, 111.97, 48.41 ppm. MS (ESI+, CH_3CN): *m/z* 1177.2761 [M−PF_6]$^+$; elemental analysis calcd (%) for $C_{60}H_{38}F_{12}IrN_8P$: C, 54.50; H, 2.90; N, 8.47. Found: C, 54.19; H, 2.84; N, 8.23 (%).

Compound 4: Reddish solid (86%); ^{1}H NMR (400 MHz, CD_3CN): δ=9.70 (dd, J=8.0, 1.2 Hz, 2H), 8.97 (s, 2H), 8.58 (dd, J=5.2, 1.2 Hz, 2H), 8.25–8.22 (m, 2H), 8.03 (dd, J=8, 5.2 Hz, 2H), 7.75 (d, J=8.0 Hz, 2H), 7.69 (d, J=8.0 Hz, 4H), 7.64–7.62 (m, 2H), 7.53 (d, J=8.0 Hz, 2H), 7.34 (d, J=8.0 Hz, 4H), 7.20 (t, J=7.6 Hz, 2H), 7.01 (t, J=6.8 Hz, 2H), 6.92–6.88 (m, 4H), 6.54 (d, J=7.6, 2H), 6.14 (br s, NCH_2Ar, 4H), 5.83 ppm (d, J=8.0 Hz, 2H); ^{13}C NMR (75.4 MHz, CD_3CN): δ=164.42, 154.32, 152.36, 151.94, 141.50, 141.24, 139.91, 139.31, 136.50, 136.15, 135.92, 134.82, 134.46, 131.86, 131.63, 130.70, 129.41, 129.26, 129.02, 127.77, 126.96, 126.76, 125.68, 125.01, 123.69, 115.18, 112.14, 48.53 ppm; MS (ESI+, CH_3CN): *m/z* 1227.2871 [M−PF_6]$^+$; elemental analysis calcd (%) for $C_{64}H_{40}F_{12}IrN_8P$: C 56.02, H 2.94, N 8.17; found: C 55.86, H 2.93, N 7.91.

Compound 5: Orange solid (83%); ^{1}H NMR (400 MHz, CD_3CN): δ=9.75 (d, J=8.4 Hz, 2H), 8.54 (dd, J=4.8, 1.2 Hz, 2H), 8.04 (dd, J=8.24, 5.16 Hz, 2H), 7.75 (s, 2H), 7.73 (d, J=8.0 Hz, 2H), 7.67 (d, J=8.0 Hz, 4H), 7.53 (d, J=8 Hz, 2H), 7.31 (d, J=8.0 Hz, 4H), 7.17 (t, J=8.0 Hz, 2H), 6.98 (t, J=7.6 Hz, 2H), 6.89 (t, J=7.6 Hz, 2H), 6.80 (t, J=8.0 Hz, 2H), 6.51 (d, J=7.6 Hz, 2H), 6.13 (br s, NCH_2Ar, 4H), 5.70 ppm (d, J=8.4 Hz, 2H); ^{13}C NMR (75.4 MHz, CD_3CN): δ=164.44, 156.11, 153.48, 152.62, 150.63, 141.60, 141.23, 139.90, 137.96, 136.47, 135.49, 134.46, 131.58, 128.66, 127.768, 127.768, 127.63, 126.93, 125.57, 125.57, 124.95, 115.06, 112.10, 105.09, 48.53 ppm. MS (ESI+, CH_3CN): *m/z* 1233.2779 [M−PF_6]$^+$; elemental analysis calcd (%) for $C_{61}H_{38}F_{12}IrN_{10}OP$: C 53.16, H 2.78, N 10.16; found: C 52.98, H 2.73, N 9.90.

X-ray crystal-structure analysis

Single crystals suitable for X-ray diffraction analysis were obtained for complex **2** from CH_2Cl_2/hexane and for complex **3** from 1,2-

$C_2H_4Cl_2$/hexane. A summary of the crystal data collection and refinement parameters for all compounds are given in Tables S3–S8. Crystals were mounted on glass fibers and transferred to the cold gas stream of a Bruker Smart APEX diffractometer. Data were recorded with $Mo_{K\alpha}$ radiation ($\lambda = 0.71073$ Å) in ω scan mode. Absorption correction for the compound was based on multiscans. Both structures were solved by direct methods (SHELXS-97[44]); refinement was done by full-matrix least squares on F^2 by using the SHELXL-97 program suite;[44] empirical (multiscan) absorption correction with SADABS (Bruker).[45] All non-hydrogen positions were refined with anisotropic temperature factors. Hydrogen atoms for aromatic CH and aliphatic CH_2 and CH_3 groups were positioned geometrically (C–H 0.95 Å for aromatic CH, C–H 0.99 Å for CH_2, C–H 0.98 Å for CH_3) and were refined by using a riding model (AFIX 43 for aromatic CH, AFIX 23 for CH_2, AFIX 137 for CH_3), with $U_{iso}(H) = 1.2\,U_{eq}$(CH, CH_2) and $U_{iso}(H) = 1.5\,U_{eq}(CH_3)$. Graphics were drawn with DIAMOND (version 4) [*DIAMOND 4* for Windows; Crystal Impact Gbr, B, 2016, Germany, http://www.crystalimpact.com/diamond]. The structural data was deposited with the Cambridge Crystallographic Data Center.[46]

Special features for 2: The *R* values were good, and the structure of the iridium cation could be unequivocally defined together with the hexafluorophosphate anions. The iridium cation crystallized with one PF_6 anion and about 1.75 methylene chloride solvent molecules. The largest seven residual electron density peaks from 2.84 to 1.71 e Å^{-3} were within 1.75 Å from the chlorine atoms of the CH_2Cl_2 solvent molecules. This is indicative of a disorder of the solvent molecules within the solvent-occupied voids between the complex molecules. The expected rotational disorder in the trifluoromethyl groups and the orientation disorder in the solvent molecules were not refined further.

Special features for 3: The largest residual electron density peak of 3.23 e Å^{-3} was within 0.88 Å from the iridium atom. The next four residual electron density peaks from 2.20 to 1.34 e Å^{-3} were within 1.26 to 0.50 Å from the chlorine atoms of the $C_2H_4Cl_2$ solvent molecules. This indicated a disorder of the solvent molecules within the solvent-occupied voids between the complex molecules. The presumable hexane solvent molecule was quite strongly disordered and could not be refined to a reasonable structure. Therefore, the electron density of the hexane solvent was treated with the SQUEEZE option in PLATON.[21] PLATON calculated/squeezed a void electron count of 46 electrons in each of the two void volumes of 141 and 145 Å^3 per unit cell volume of 3277 Å^3. The electron count of a hexane molecule is 48. With $Z = 2$ there was then one hexane molecule per crystal formula unit. The *R* values were good, and the structure of the iridium cation could be unequivocally defined together with the hexafluorophosphate anion and the 2.375 1,2-dichloroethane solvent molecules. The expected rotational disorder in the trifluoromethyl groups and the orientation disorder in the solvent molecules were not refined further.

Photophysical measurements

UV/Vis spectroscopy was performed with a PerkinElmer Lambda 750 S spectrometer with operating software. Emission spectra were obtained with a Horiba Jobin Yvon Fluorolog 3–22 modular spectrofluorometer with a 450 W xenon lamp. Measurements were performed in a right-angle configuration by using 10 mm quartz fluorescence cells for solutions at 298 K. Emission lifetimes (τ) were measured by using an IBH FluoroHub TCSPC controller and a NanoLED pulse diode excitation source ($\tau < 10$ µs); the estimated uncertainty was ±10% or better. Emission quantum yields (Φ) were measured by using a Hamamatsu C11347 Absolute PL Quantum Yield Spectrometer; the estimated uncertainty was ±5% or better. H_2O/DMSO solutions of the samples were previously degassed by bubbling argon for 30 min.

RP-HPLC purity and stability analyses

The purity of the Ir^{III} complexes was analyzed by using a RP-HPLC/MS TOF 6220 equipped with a double binary pump (model G1312A), degasser, autosampler (model G1329A), diode array detector (model G1315D), and mass detector in series (Agilent Technologies 1200). Chromatographic analyses were performed with a Brisa C18 column (150 mm × 4.6 mm, 5 µm particle size); Teknokroma, Macclesfield, UK. The mobile phase was a mixture of (A) H_2O/HCOOH 0.1% and (B) acetonitrile/HCOOH 0.1%. The flow rate was 0.6 mL min^{-1} in a linear gradient (see Table S1 for the gradient used). Chromatograms were recorded at $\lambda = 280$ nm. The HPLC system was controlled by a ChemStation software (MASS HUNTER). The mass detector was an ion-trap spectrometer equipped with a dual-source electrospray APCI. Mass spectrometry data were acquired in the positive ionization mode. The ionization conditions were adjusted at 350 °C and 3 kV for capillary temperature and voltage, respectively. The nebulizer pressure and flow rate of nitrogen were 60 psi and 12 L min^{-1}, respectively. The full scan mass covered the range of *m/z* 100 to 1000. Samples were dissolved in DMSO (50 µM final concentration).

Photostability

A H_2O/DMSO solution of **3** was prepared, and its UV/Vis spectra were recorded. The sample in the cuvette was irradiated at $\lambda =$ 420 nm for 15 min with a 450 W xenon lamp. After this time, the UV/Vis spectrum was collected again.

Transmission electron microscopy

TEM experiments were performed with a PHILIPS TECNAI 12 transmission electron microscope and JEOL 1011 transmission electron microscope. The samples were prepared by dropping a few drops of H_2O/DMSO (99:1) solution onto a carbon-coated nickel grid. Slow evaporation of solvents in the air for 10 min was allowed before placing the samples into the sample chamber of the instrument.

Cell lines

The human ovarian carcinoma cell lines A2780 (cisplatin sensitive) and A2780cisR (a cisplatin-resistant variant of A2780) as well as human breast cancer MCF-7 cells were kindly supplied by Professor B. Keppler, University of Vienna (Austria). Human cervix adenocarcinoma HeLa cells were obtained from ECACC. MCF-10 (nonmalignant mammary gland cells) were obtained from ATCC. The A2780 and A2780cisR cells were grown in RPMI 1640 medium supplemented with gentamycin (50 µg mL^{-1}) and 10% heat-inactivated fetal bovine serum. The acquired resistance of A2780cisR cells was maintained by supplementing the medium with 1 µM cisplatin every second passage. The MCF-7, HeLa, and MCF-10A cells were grown in DMEM (high glucose, 4.5 g L^{-1}) supplemented with gentamycin (50 µg mL^{-1}) and 10% heat-inactivated fetal bovine serum. The medium for MCF-10A cells was supplemented with 100 ng mL^{-1} cholera toxin. The cells were cultured in a humidified incubator at 37 °C under a 5% CO_2 atmosphere and were subcultured 2–3 times a week with an appropriate plating density.

In vitro growth inhibition assay

The cytotoxic activity of the investigated Ir complexes and cisplatin was determined against the human ovarian carcinoma cell lines A2780 and A2780cisR, human cervix adenocarcinoma (HeLa), and human breast adenocarcinoma (MCF7) cell line. Cells were seeded on 96-well tissue culture plates at a density of 10^4 cells per well for A2780 and A2780R cells and 5×10^3 cells per well for HeLa and MCF7 cells in growth medium (100 μL) and were incubated at 37 °C in a humidified 5% CO_2 atmosphere for 16 h. After the incubation period, the cells were treated with the compounds and kept in the incubator for an additional 72 h. The stock solutions of the metal-based compounds were always freshly prepared in DMSO before use. The final concentration of DMSO in the cell-culture medium did not exceed 0.1% (*v/v*), which was shown not to affect cell growth. The final concentrations of the tested compounds were in the range of 0 to 50 μM in a volume of 200 μL per well. Subsequently, MTT solution (5 mg mL^{-1}, 10 μL) was added to each well, and plates were incubated for 4 h. At the end of the incubation time, the medium was removed, and the formazan product was dissolved in DMSO (100 μL per well). Cell viability was evaluated by measuring the absorbance at $\lambda=570$ nm (reference wavelength at 630 nm) by using an absorbance reader Synergy Mx (Biotek, USA). IC_{50} values were calculated from curves constructed by plotting cell survival [%] versus drug concentration [μM]. The reading values were converted into the percentage of control [% cell survival]. Cytotoxic effects were expressed as IC_{50}. All experiments were done in triplicate.

DNA interactions in cell-free media

Interactions of the investigated Ir complexes with naked DNA were studied by various biophysical and biochemical methods, described in the Supporting Information in detail.

Cellular accumulation

Cellular accumulation of Ir compounds and cisplatin was determined in HeLa cells. The cells were seeded on 100 mm tissue culture dishes (1.5×10^6 cells per dish in 8 mL of growth medium). After 48 h of incubation, the cells were treated with tested compounds at equimolar concentrations (10 μM) for 5 or 24 h. The attached cells were harvested by trypsinization, and the cell pellets were washed with cold PBS (phosphate-buffered saline) twice. The pellets were digested by using a microwave acid (HCl, 11 M) digestion system (MARS5, CEM) to give a fully homogenized solution. Final iridium and platinum contents in the samples were determined by ICP-MS.

Localization of Ir complexes in cells by confocal microscopy

HeLa cells were seeded on 35 mm glass-bottomed confocal culture dishes (Mattek Co., MA, USA) at a density of 2×10^5 cells per dish and were incubated overnight. The next day, cells were treated with tested compounds (1 μM) for 24 h and were then analyzed with a confocal laser-scanning microscope Leica TCS SP8 SMD (Leica microsystems GmbH, Wetzlar, Germany). Samples were excited at $\lambda=405$ nm, and the detection window was set from $\lambda=520$ to 610 nm.

Detection of apoptosis and necrosis

The cell-death detection ELISA plus kit (Roche Molecular Biochemicals, Mannheim, Germany) was used to determine the extent of apoptosis and necrosis in cancer cells treated with the investigated Ir complexes. In this assay, internucleosomal DNA fragmentation was quantitatively assayed by antibody-mediated capture and detection of cytoplasmic mononucleosome- and oligonucleosome-associated histone–DNA complexes. HeLa cells were treated with equitoxic concentrations of Ir complexes corresponding to their IC_{20}, IC_{50}, and IC_{80} values determined after 72 h in these cells (0.36, 1.76, and 4.68 μM for **1**; 7.6, 23, and 36 μM for **5**). Then, the cells were centrifuged (300 *g*, 10 min), and the experiment was performed as already described[47] according to the manufacturer's protocol. Following incubation with peroxidase substrate for 20 min, absorbance was determined at $\lambda=405$ nm (reference wavelength 492 nm) with a microplate reader (absorbance reader Sunrise Tecan Schoeller). Signals from wells containing the substrate only were subtracted as background. Other details of this assay and data analysis were performed according to the manufacturer's instructions.

Real-time cell electronic sensing

The real-time cell analyzer (RTCA) equipment (xCELLigence RTCA SP instrument, Roche) was calibrated for the background impedance with fresh RPMI 1640 medium (100 μL). A2780 cells and HeLa cells were added at a density of 8000 and 4000 cells per well, respectively, and were incubated for 24 h at 37 °C under a humidified 5% CO_2 atmosphere. Subsequently, the cells were treated with tested compounds. Cell-sensor impedance called the cell index is defined as [Eq. (1)]:

$$\text{Cell index} = \frac{(R_t - R_b)}{15} \quad (1)$$

in which R_t is the impedance of the cells at defined time points, and R_b is the background impedance of the culture medium. Impedance was monitored for 5 min sweeps for the duration of the experiment. Cell index was normalized at the time of treatment (24 h). Each sample was plated on the E-plate as quadruplicate. The concentrations of treated compounds in the media used for treatment were verified by flameless atomic absorption spectroscopy (FAAS).

Effect on protein and RNA synthesis in cells

HeLa cells were seeded in 6-well plates (5×10^3 cells per well) and were grown for 24 h. The medium was replaced with fresh medium with the absence and/or presence of iridium compounds, and the cells were incubated for 1 h. The medium was removed, and the cells were washed with PBS (2×) and were incubated in medium containing [^{35}S]-Met (5 μCi per sample) for 2 h. The negative control sample was incubated without [^{35}S]-Met. The medium was removed, and the cells were washed with PBS (3×), trypsinized, counted, and pelleted. Cell pellets were lysed in ice-cold radio immunoprecipitation assay (RIPA) buffer (1 mL/30 min). The lysates were cleared by centrifugation (15000 *g*/15 min). Individual lysates (40 μL) were transferred onto a 0.22 μm filter and were washed with 5% trifluoroacetic acid (TFA) thrice. The samples were analyzed by using a Scintillation analyzer (Tri-Carb 2800TR, PerkinElmer).

Co-localization of Ir complexes in cells by confocal microscopy

HeLa cells were seeded on 35 mm glass-bottomed confocal culture dishes (Mattek Co., MA, USA) at a density of 2×10^5 cells per dish and were incubated overnight. The next day, the cells were treated

with the test compounds (5 μM). After 2 h of incubation, cells were co-stained with ER-Tracker (red, BODIPY TR glibenclamide; ThermoFisher Scientific, Waltham, MA, USA) at a concentration of 1 μM and were then analyzed with a confocal laser-scanning microscope Leica TCS SP8 SMD (Leica microsystems GmbH, Wetzlar, Germany). The investigated Ir complexes were excited at $\lambda = 405$ nm, and ER-Tracker was excited at $\lambda = 587$ nm. Samples were scanned sequentially, and the emission parameters were carefully set to omit possible fluorescence overlaps. Co-localization analysis was performed as described previously[35] by the use of the Coloc2 plugin in ImageJ software. Briefly, the Pearson coefficient of correlation (PCC) was measured for entire images by default, and the Costes regression method for estimation of the threshold was used. Values of PCC are expressed as the mean ± SD above the calculated threshold.

Phototoxicity testing

The phototoxic activity of the investigated Ir complexes was determined against HeLa cells. Cells were seeded on 96-well tissue-culture plates at a density of 5×10^3 cells per well in growth medium (100 μL) and were left to adhere at 37 °C under a humidified 5% CO_2 atmosphere for 24 h. After washing cells with PBS, the tested compounds were added in EBSS and were incubated for 1 h under cultivation conditions. After the incubation period, cells were irradiated by visible light for 1 h ($\lambda_{max} = 420$ nm) in the presence of the tested compounds. Subsequently, EBSS with the compound was removed, and cells were washed with PBS and then returned to the incubator in complete DMEM. Nonirradiated controls were tested as well. The stock solutions of compounds were always freshly prepared in DMSO before use. The final concentration of DMSO in cell-culture medium did not exceed 0.1% (*v/v*), which was shown not to affect cell growth. The final concentrations of the tested compounds were in the range of 0 to 100 μM in a volume of 200 μL per well. The phototoxicity was determined 70 h after irradiation by using the standard MTT assay. Briefly, MTT solution (5 mg mL^{-1}, 10 μL) was added to each well, and plates were incubated for 4 h. At the end of the incubation time, the medium was removed, and the formazan product was dissolved in DMSO (100 μL per well). Cell viability was evaluated by measuring the absorbance at $\lambda = 570$ nm (reference wavelength at 630 nm) by using an absorbance reader Synergy Mx (Biotek, USA).The IC_{50} values were calculated from curves constructed by plotting cell survival [%] versus drug concentration [μM]. All experiments were done in triplicate. The reading values were converted into the percentage of control [% cell survival]. Phototoxic effects were expressed as IC_{50}.

Determination of intracellular reactive oxygen species (ROS)

To determine the oxidative stress induced by the investigated Ir complexes, intracellular ROS were quantified in HeLa cells. Cells were seeded on 96-well black plates at a density of 1×10^4 cells per well and were incubated at 37 °C under a humidified 5% CO_2 atmosphere for 16 h. Subsequently, the cells were treated with tested compounds in EBSS at equimolar concentrations (1, 5, 10, and 20 μM) and were held under cultivation conditions for 1 h. Then, cells were irradiated with blue light ($\lambda_{max} = 420$ nm) for 1 h or, alternatively, were kept in the dark for this period. Afterwards, intracellular ROS were quantified by using a method developed earlier.[33b,40] Briefly, 10 μM 2′,7′-dichlorodihydrofluorescein diacetate (DCFH-DA) was added to the cells, and samples were incubated for 30 min at 37 °C. The fluorescence intensity was evaluated by measuring the fluorescence (excitation/emission wavelengths: 504/529 nm) by using a fluorescence reader Synergy Mx (Biotek, USA). Three independent experiments were performed.

Acknowledgements

V.N., J.K., and V.B. were supported by the Czech Science Foundation (Grant 17–05302S) and Ministry of Education of the Czech Republic (Grant LTC17003). J.P. was supported by the National Program of Sustainability I (LO1204). The work of G.V., N.C., and J.R. was supported by the Spanish Ministry of Economy and Competitiveness and FEDER funds (Project CTQ2015-64319-R). The authors are also indebted to Dr. Karel Soucek from the Institute of Biophysics, Czech Academy of Sciences, Brno for enabling them to use RTCA equipment (xCELLigence RTCA SP, Roche). G.V. thanks the University of Murcia for a grant (R-1034/2016). The authors also thank the members of the COST Action CM1406 and MetDrugs network (CTQ2015-70371-REDT) for stimulating discussions.

Conflict of interest

The authors declare no conflict of interest.

Keywords: anticancer agents · cell growth · conjugation · iridium · protein design

[1] a) D. Wang, S. J. Lippard, *Nat. Rev. Drug Discovery* **2005**, *4*, 307–320; b) L. Kelland, *Nat. Rev. Cancer* **2007**, *7*, 573–584; c) N. Muhammad, Z. Guo, *Curr. Opin. Chem. Biol.* **2014**, *19*, 144–153.

[2] a) Z. Liu, P. J. Sadler, *Acc. Chem. Res.* **2014**, *47*, 1174–1185; b) J. M. Hearn, I. Romero-Canelon, B. Qamar, Z. Liu, I. Hands-Portman, P. J. Sadler, *ACS Chem. Biol.* **2013**, *8*, 1335–1343; c) C. Yang, W. H. Wang, G. D. Li, H. J. Zhong, Z. Z. Dong, C. Y. Wong, D. W. J. Kwong, D. L. Ma, C. H. Leung, *Sci. Rep.* **2017**, *7*, 42860; d) R. J. Needham, C. Sanchez-Cano, X. Zhang, I. Romero-Canelón, A. Habtemariam, M. S. Cooper, L. Meszaros, G. J. Clarkson, P. J. Blower, P. J. Sadler, *Angew. Chem. Int. Ed.* **2017**, *56*, 1017–1020; *Angew. Chem.* **2017**, *129*, 1037–1040; e) A. Wilbuer, D. H. Vlecken, D. J. Schmitz, K. Kraling, K. Harms, C. P. Bagowski, E. Meggers, *Angew. Chem. Int. Ed.* **2010**, *49*, 3839–3842; *Angew. Chem.* **2010**, *122*, 3928–3932; f) C. M. Hackl, M. S. Legina, V. Pichler, M. Schmidlehner, A. Roller, O. Dömötör, E. A. Enyedy, M. A. Jakupec, W. Kandioller, B. K. Keppler, *Chem. Eur. J.* **2016**, *22*, 17269–17281; g) G. Gasser, I. Ott, N. Metzler-Nolte, *J. Med. Chem.* **2011**, *54*, 3–25; h) Z. Adhireksan, G. E. Davey, P. Campomanes, M. Groessl, C. M. Clavel, H. Yu, A. A. Nazarov, C. H. F. Yeo, W. H. Ang, P. Dröge, U. Rothlisberger, P. J. Dyson, C. A. Davey, *Nat. Commun.* **2014**, *5*, 3462; i) J. Ruiz, C. Vicente, C. de Haro, D. Bautista, *Inorg. Chem.* **2013**, *52*, 974–982; j) N. Cutillas, G. S. Yellol, C. de Haro, C. Vicente, V. Rodríguez, J. Ruiz, *Coord. Chem. Rev.* **2013**, *257*, 2784–2797; k) M. J. Chow, M. Alfiean, G. Pastorin, C. Gaiddon, W. H. Ang, *Chem. Sci.* **2017**, *8*, 3641–3649; l) G. Gasser, N. Metzler-Nolte, *Curr. Opin. Chem. Biol.* **2012**, *16*, 84–91.

[3] a) L. J. Liu, W. H. Wang, S. Y. Huang, Y. J. Hong, G. D. Li, S. Lin, J. L. Tian, Z. W. Cai, H. M. D. Wang, D. L. Ma, C. H. Leung, *Chem. Sci.* **2017**, *8*, 4756–4763; b) H. J. Zhong, L. H. Lu, K. H. Leung, C. C. L. Wong, C. Peng, S. C. Yan, D. L. Ma, Z. W. Cai, H. M. D. Wang, C. H. Leung, *Chem. Sci.* **2015**, *6*, 5400–5408.

[4] R. Cao, J. L. Jia, X. C. Ma, M. Zhou, H. Fei, *J. Med. Chem.* **2013**, *56*, 3636–3644.

[5] a) J. J. Cao, C. P. Tan, M. H. Chen, N. Wu, D. Y. Yao, X. G. Liu, L. N. Ji, Z. W. Mao, *Chem. Sci.* **2017**, *8*, 631–640; b) F. X. Wang, M. H. Chen, Y. N. Lin, H. Zhang, C. P. Tan, L. N. Ji, Z. W. Mao, *ACS Appl. Mater. Interfaces* **2017**, *9*, 42471–42481.

[6] I. Gamba, I. Salvado, R. F. Brissos, P. Gamez, J. Brea, M. I. Loza, M. E. Vazquez, M. V. Lopez, *Chem. Commun.* **2016**, *52*, 1234 – 1237.
[7] a) V. Novohradsky, A. Zamora, A. Gandioso, V. Brabec, J. Ruiz, V. Marchan, *Chem. Commun.* **2017**, *53*, 5523 – 5526; b) X. C. Ma, J. L. Jia, R. Cao, X. B. Wang, H. Fei, *J. Am. Chem. Soc.* **2014**, *136*, 17734 – 17737.
[8] a) C. Y. Li, M. X. Yu, Y. Sun, Y. Q. Wu, C. H. Huang, F. Y. Li, *J. Am. Chem. Soc.* **2011**, *133*, 11231 – 11239; b) Y. You, S. Lee, T. Kim, K. Ohkubo, W. S. Chae, S. Fukuzumi, G. J. Jhon, W. Nam, S. J. Lippard, *J. Am. Chem. Soc.* **2011**, *133*, 18328 – 18342; c) Y. You, Y. Han, Y. M. Lee, S. Y. Park, W. Nam, S. J. Lippard, *J. Am. Chem. Soc.* **2011**, *133*, 11488 – 11491; d) K. K.-S. Tso, K. K.-W. Lo, in *Iridium(III) in Optoelectronic and Photonics Applications* (Ed.: E. Zysman-Colman), Wiley, Chichester, **2017**, https://doi.org/10.1002/9781119007166.ch9, pp. 415 – 477; e) L. C. C. Lee, J. C. W. Lau, H. W. Liu, K. K. W. Lo, *Angew. Chem. Int. Ed.* **2016**, *55*, 1046 – 1049; *Angew. Chem.* **2016**, *128*, 1058 – 1061.
[9] C. Mari, H. Y. Huang, R. Rubbiani, M. Schulze, F. Wurthner, H. Chao, G. Gasser, *Eur. J. Inorg. Chem.* **2017**, 1745 – 1752.
[10] I. Yoon, J. Z. Li, Y. K. Shim, *Clin. Endosc.* **2013**, *46*, 7 – 23.
[11] Y. Chen, R. L. Guan, C. Zhang, J. J. Huang, L. N. Ji, H. Chao, *Coord. Chem. Rev.* **2016**, *310*, 16 – 40.
[12] a) C. Mari, V. Pierroz, S. Ferrari, G. Gasser, *Chem. Sci.* **2015**, *6*, 2660 – 2686; b) E. C. Glazer, *Isr. J. Chem.* **2013**, *53*, 391 – 400.
[13] a) M. Stephenson, C. Reichardt, M. Pinto, M. Wachtler, T. Sainuddin, G. Shi, H. Yin, S. Monro, E. Sampson, B. Dietzek, S. A. McFarland, *J. Phys. Chem. A* **2014**, *118*, 10507 – 10521; b) C. Reichardt, K. R. A. Schneider, T. Sainuddin, M. Waechtler, S. A. McFarland, B. Dietzek, *J. Phys. Chem. A* **2017**, *121*, 5635 – 5644.
[14] a) J. S. Nam, M.-G. Kang, J. Kang, S.-Y. Park, S. J. C. Lee, H.-T. Kim, J. K. Seo, O.-H. Kwon, M. H. Lim, H.-W. Rhee, T.-H. Kwon, *J. Am. Chem. Soc.* **2016**, *138*, 10968 – 10977; b) K. Q. Qiu, M. Ouyang, Y. K. Liu, H. Y. Huang, C. F. Liu, Y. Chen, L. N. Ji, H. Chao, *J. Mater. Chem. B* **2017**, *5*, 5488 – 5498; c) X. H. Tian, Y. Z. Zhu, M. Z. Zhang, L. Luo, J. Y. Wu, H. P. Zhou, L. J. Guan, G. Battaglia, Y. P. Tian, *Chem. Commun.* **2017**, *53*, 3303 – 3306.
[15] M. A. Baldo, M. E. Thompson, S. R. Forrest, *Nature* **2000**, *403*, 750 – 753.
[16] J. B. Waern, C. Desmarets, L. M. Chamoreau, H. Amouri, A. Barbieri, C. Sabatini, B. Ventura, F. Barigelletti, *Inorg. Chem.* **2008**, *47*, 3340 – 3348.
[17] a) Y. You, *Curr. Opin. Chem. Biol.* **2013**, *17*, 699 – 707; b) R. M. Gao, D. G. Ho, B. Hernandez, M. Selke, D. Murphy, P. I. Djurovich, M. E. Thompson, *J. Am. Chem. Soc.* **2002**, *124*, 14828 – 14829.
[18] a) B. Mariana, G. Mercedes, *Mini-Rev. Med. Chem.* **2005**, *5*, 409 – 424; b) Y. Bansal, O. Silakari, *Bioorg. Med. Chem.* **2012**, *20*, 6208 – 6236.
[19] a) G. S. Yellol, A. Donaire, J. G. Yellol, V. Vasylyeva, C. Janiak, J. Ruiz, *Chem. Commun.* **2013**, *49*, 11533 – 11535; b) J. Yellol, S. A. Perez, A. Buceta, G. Yellol, A. Donaire, P. Szumlas, P. J. Bednarski, G. Makhloufi, C. Janiak, A. Espinosa, J. Ruiz, *J. Med. Chem.* **2015**, *58*, 7310 – 7327; c) J. Yellol, S. A. Pérez, G. Yellol, J. Zajac, A. Donaire, G. Vigueras, V. Novohradsky, C. Janiak, V. Brabec, J. Ruiz, *Chem. Commun.* **2016**, *52*, 14165 – 14168; d) V. Novohradsky, J. Yellol, O. Stuchlikova, M. D. Santana, H. Kostrhunova, G. Yellol, J. Kasparkova, D. Bautista, J. Ruiz, V. Brabec, *Chem. Eur. J.* **2017**, *23*, 15294 – 15299.
[20] G. S. Yellol, J. G. Yellol, V. B. Kenche, X. M. Liu, K. J. Barnham, A. Donaire, C. Janiak, J. Ruiz, *Inorg. Chem.* **2015**, *54*, 470 – 475.
[21] A. L. Spek, *Acta Crystallogr. Sect. D* **2009**, *65*, 148 – 155.
[22] a) J. Ruiz, V. Rodriguez, C. de Haro, A. Espinosa, J. Perez, C. Janiak, *Dalton Trans.* **2010**, *39*, 3290 – 3301; b) J. Ruiz, M. D. Villa, V. Rodriguez, N. Cutillas, C. Vicente, G. Lopez, D. Bautista, *Inorg. Chem.* **2007**, *46*, 5448 – 5449; c) G. Althoff, J. Ruiz, V. Rodriguez, G. Lopez, J. Perez, C. Janiak, *CrystEngComm* **2006**, *8*, 662 – 665; d) A. Zamora, S. A. Pérez, V. Rodríguez, C. Janiak, G. S. Yellol, J. Ruiz, *J. Med. Chem.* **2015**, *58*, 1320 – 1336.
[23] a) M. Nishio, *Phys. Chem. Chem. Phys.* **2011**, *13*, 13873 – 13900; b) M. Nishio, Y. Umezawa, K. Honda, S. Tsuboyama, H. Suezawa, *CrystEngComm* **2009**, *11*, 1757 – 1788; c) M. Nishio, *CrystEngComm* **2004**, *6*, 130 – 158; d) C. Janiak, S. Temizdemir, S. Dechert, W. Deck, F. Girgsdies, J. Heinze, M. J. Kolm, T. G. Scharmann, O. M. Zipffel, *Eur. J. Inorg. Chem.* **2000**, 1229 – 1241; e) U. Yoji, T. Sei, H. Kazumasa, U. Jun, N. Motohiro, *Bull. Chem. Soc. Jp.* **1998**, *71*, 1207 – 1213.
[24] a) X. J. Yang, F. Drepper, B. Wu, W. H. Sun, W. Haehnel, C. Janiak, *Dalton Trans.* **2005**, 256 – 267; b) C. Janiak, *J. Chem. Soc. Dalton Trans.* **2000**, 3885 – 3896.
[25] a) Y. Hisamatsu, A. Shibuya, N. Suzuki, T. Suzuki, R. Abe, S. Aoki, *Bioconjugate Chem.* **2015**, *26*, 857 – 879; b) L. He, J. Qiao, L. Duan, G. F. Dong, D. Q. Zhang, L. D. Wang, Y. Qiu, *Adv. Funct. Mater.* **2009**, *19*, 2950 – 2960.
[26] K. K. W. Lo, *Acc. Chem. Res.* **2015**, *48*, 2985 – 2995.
[27] a) M. N. Huang, R. N. Yu, K. Xu, S. X. Ye, S. Kuang, X. H. Zhu, Y. Q. Wan, *Chem. Sci.* **2016**, *7*, 4485 – 4491; b) B. Blondel, F. Delarue, M. Lopes, S. Ladeira-Mallet, F. Alary, C. Renaud, I. Sasaki, *Synth. Met.* **2017**, *227*, 106 – 116; c) L. Y. Zong, Y. J. Xie, C. Wang, J. R. Li, Q. Q. Li, Z. Li, *Chem. Commun.* **2016**, *52*, 11496 – 11499.
[28] a) E. Y. H. Hong, H. L. Wong, V. W. W. Yam, *Chem. Commun.* **2014**, *50*, 13272 – 13274; b) E. Y. H. Hong, H. L. Wong, V. W. W. Yam, *Chem. Eur. J.* **2015**, *21*, 5732 – 5735.
[29] V. Brabec, O. Hrabina, J. Kasparkova, *Coord. Chem. Rev.* **2017**, *351*, 2 – 31.
[30] V. Brabec, O. Novakova, *Drug Resist. Updates* **2006**, *9*, 111 – 122.
[31] K. Y. Zhang, S. P. Y. Li, N. Y. Zhu, I. W. S. Or, M. S. H. Cheung, Y. W. Lam, K. K. W. Lo, *Inorg. Chem.* **2010**, *49*, 2530 – 2540.
[32] a) S. A. Pérez, C. de Haro, C. Vicente, A. Donaire, A. Zamora, J. Zajac, H. Kostrhunova, V. Brabec, D. Bautista, J. Ruiz, *ACS Chem. Biol.* **2017**, *12*, 1524 – 1537; b) A. Zamora, S. A. Pérez, M. Rothemund, V. Rodríguez, R. Schobert, C. Janiak, J. Ruiz, *Chem. Eur. J.* **2017**, *23*, 5614 – 5625.
[33] a) Y. A. Abassi, B. Xi, W. F. Zhang, P. F. Ye, S. L. Kirstein, M. R. Gaylord, S. C. Feinstein, X. B. Wang, X. Xu, *Chem. Biol.* **2009**, *16*, 712 – 723; b) V. Novohradsky, L. Zerzankova, J. Stepankova, A. Kisova, H. Kostrhunova, Z. Liu, P. J. Sadler, J. Kasparkova, V. Brabec, *Metallomics* **2014**, *6*, 1491 – 1501.
[34] a) A. P. Grollman, *J. Biol. Chem.* **1967**, *242*, 3226 – 3233; b) F. Van Coppenolle, F. V. Abeele, C. Slomianny, M. Flourakis, J. Hesketh, E. Dewailly, N. Prevarskayal, *J. Cell Sci.* **2004**, *117*, 4135 – 4142; c) N. Garreau de Loubresse, I. Prokhorova, W. Holtkamp, M. V. Rodnina, G. Yusupova, M. Yusupov, *Nature* **2014**, *513*, 517 – 522.
[35] K. W. Dunn, M. M. Kamocka, J. H. McDonald, *Am. J. Physiol. Cell Physiol.* **2011**, *300*, C723 – C742.
[36] a) U. Fischer, K. Schulze-Osthoff, *Cell Death Differ.* **2005**, *12*, 942 – 961; b) J. A. Hickman, *Cancer Metastasis Rev.* **1992**, *11*, 121 – 139.
[37] a) V. Cepero, B. Garcia-Serrelde, V. Moneo, F. Blanco, A. M. Gonzalez-Vadillo, A. Alvarez-Valdes, C. Navarro-Ranninger, A. Carnero, *Clin. Trans. Oncol.* **2007**, *9*, 521 – 530; b) R. J. Ernst, A. C. Komor, J. K. Barton, *Biochemistry* **2011**, *50*, 10919 – 10928; c) K. Suntharalingam, S. G. Awuah, P. M. Bruno, T. C. Johnstone, F. Wang, W. Lin, Y.-R. Zheng, J. E. Page, M. T. Hemann, S. J. Lippard, *J. Am. Chem. Soc.* **2015**, *137*, 2967 – 2974.
[38] Y. Li, B. Liu, X.-R. Lu, M.-F. Li, L.-N. Ji, Z.-W. Mao, *Dalton Trans.* **2017**, *46*, 11363 – 11371.
[39] F. W. Shao, B. Elias, W. Lu, J. K. Barton, *Inorg. Chem.* **2007**, *46*, 10187 – 10199.
[40] a) J. P. Robinson, L. H. Bruner, C. F. Bassoe, J. L. Hudson, P. A. Ward, S. H. Phan, *J. Leukocyte Biol.* **1988**, *43*, 304 – 310; b) B. Kalyanaraman, V. Darley-Usmar, K. J. A. Davies, P. A. Dennery, H. J. Forman, M. B. Grisham, G. E. Mann, K. Moore, L. J. Roberts, H. Ischiropoulos, *Free Radical Biol. Med.* **2012**, *52*, 1 – 6.
[41] P. M. Bruno, Y. Liu, G. Y. Park, J. Murai, C. E. Koch, T. J. Eisen, J. R. Pritchard, Y. Pommier, S. J. Lippard, M. T. Hemann, *Nat. Med.* **2017**, *23*, 461 – 471.
[42] Z. Molphy, A. Prisecaru, C. Slator, N. Barron, M. McCann, J. Colleran, D. Chandran, N. Gathergood, A. Kellett, *Inorg. Chem.* **2014**, *53*, 5392 – 5404.
[43] J. L. Yao, X. Gao, W. L. Sun, S. Shi, T. M. Yao, *Dalton Trans.* **2013**, *42*, 5661 – 5672.
[44] G. M. Sheldrick, *Acta Crystallogr. Sect. A* **2008**, *64*, 112 – 122.
[45] G. M. Sheldrick, SADABS, Program for empirical absorption correction of area detector data, University of Göttingen, Germany, 1996, Universität Göttingen, Göttingen, **1996**.
[46] CCDC 1584720 (**2**) and 1584721 (**3**) contain the supplementary crystallographic data for this paper. These data are provided free of charge by The Cambridge Crystallographic Data Centre.
[47] A. Kisova, L. Zerzankova, A. Habtemariam, P. J. Sadler, V. Brabec, J. Kasparkova, *Mol. Pharm.* **2011**, *8*, 949 – 957.

Manuscript received: November 12, 2017
Accepted manuscript online: January 25, 2018
Version of record online: February 27, 2018